

# Development of Large Strain Shell Elements for Woven Fabrics with Application to Clothing Pressure Distribution Problem

M. Tanaka<sup>1,2</sup>, H. Noguchi<sup>1</sup>, M. Fujikawa<sup>3,4</sup>, M. Sato<sup>3</sup>, S. Oi<sup>3</sup>  
T. Kobayashi<sup>3</sup>, K. Furuichi<sup>5</sup>, S. Ishimaru<sup>5</sup> and C. Nonomura<sup>5</sup>

**Abstract:** This paper describes the development of a proper constitutive model of woven fabrics and its implementation in nonlinear finite shell elements in order to simulate the large deformation behavior of cloth. This work currently focuses on a macroscopic continuum constitutive model that is capable of capturing the realistic mechanical behavior of cloth that is characterized by two families of yarns, i.e., warp and weft. In this study, two strategies are considered. One is a rebar layer model and the other is a polyconvex anisotropic hyperelastic material model. The latter avoids non-physical behavior and can consider the effect of the interaction between the warp and the weft, whereas the former cannot do so. These material models are implemented in a four-node shell element in Abaqus/Standard (S4R type) via the UMAT user-subroutine. These models can be used to predict the outcome of uniaxial tensile tests and compute the contact pressure exerted by clothing on the human body. The resultant pressure distribution can then be used to design a form of cloth that provides more comfortable fitting.

**Keywords:** structures; finite element method; shells; constitutive equations; anisotropy; clothing pressure

## 1 Introduction

It is crucial for most companies/firms producing/designing fabrics, fibers, and garment to incorporate some type of integrated Computer Aided Engineering (CAE) systems into their production procedures. An integrated CAE system will enable

---

<sup>1</sup> Keio University, Yokohama, JPN

<sup>2</sup> Toyota Central R & D Laboratories, Inc., Nagakute, JPN

<sup>3</sup> Mechanical Design & Analysis Corporation, Chofu, JPN

<sup>4</sup> University of the Ryukyus, Nishihara, JPN

<sup>5</sup> TOYOBO Co., Ltd., Otsu, JPN

the entire design process of products to be simulated on computers and should provide all the data required to manufacture products. Such a simulation should simplify the entire product design process, potentially reducing its time and cost by as much as 80 to 90%. Therefore, it is important to adopt a realistic simulation to efficiently design garments. However, currently available CAE systems do not possess such simulation capabilities due to some technical difficulties, despite the urgent requirement for the same. One of the main difficulties involved in constructing a desired system for designing comfortable clothing is to quantify "comfort." Clothing pressure, i.e., the contact pressure between a garment and human skin, could be one indicator that can be specifically applied to evaluate the comfort of clothing, along with other variables such as thermal characteristics, tactile sensation, and moisture transfer of fibers and textiles. In fields such as healthcare and sports, it is necessary to provide some simplified and accurate means for understanding the clothing pressure and its distribution during body movements in order to design comfortable clothing and clothing materials.

Considering the abovementioned motivations, we developed a new technique to predict the distribution of contact pressure. This paper presents material models of woven fabric derived from this work. These fabrics have fibers that are oriented in two directions, i.e., warp and weft. When the fabric is stretched in either of these directions, it exhibits different characteristics. Kwon and Roach [Kwon and Roach (2004)] developed a micromechanical unit-cell model to compute effective stiffness and strength of woven fabric composites, that could be implemented into a multi-level, multi-scale analysis technique. However, this model could describe relatively small strain deformation behavior. This study concerns with the material model of woven fabrics using the finite deformation theory of continuum mechanics, since large strains of woven fabrics happens during the clothing procedure. Therefore, two strategies to model the large strain deformation behavior of woven fabrics are developed herein. One is a rebar layer model [Ishimaru, Isogai, Matsui, Negishi, Nonomura, and Yokoyama (2009); Mesehke and Helnwein (1994)] that functions to reinforce the material in a uniaxial direction in the same manner as metal rebars are used to reinforce concrete. In this model, an isotropic neo-Hookean hyperelastic shell is used as the matrix of the material to which rebars or reinforcement are added. However, although such a model is quite easy to assemble and useful, it is not suitable for the accurate fabric modeling of the interaction between warp and weft. To overcome this issue, another material model is proposed. This model utilizes anisotropic hyperelastic shells with a polyconvex strain energy function that can capture the effect of the interaction between warp and weft, thus providing more accurate and robust fabric modeling. Hyperelasticity allows the formulation of a large deformation including the anisotropic effect by using a structural ten-

sor that consists of fiber-directional unit vectors [Holzapfel (2000); Reese, Raible, and Wriggers (2001); Lu and Zhang (2005); Markert, Ehlers, and Karajan (2005); Nedjar (2007); ten Thije, Akkerman, and Huétink (2007); Harrysson, Harrysson, and Ristinmaa (2007); Himpel, Menzel, Kuhl, and Steinmann (2007); Lu, Zhou, and Raghavan (2007); Bonet and Burton (1998)]. In order to avoid non-physical behavior, the associated strain-energy function must be polyconvex. A number of literatures on polyconvexity can be found [Schröder and Neff (2003b); Schröder, Neff, and Balzani (2005); Itskov and Aksel (2004); Markert, Ehlers, and Karajan (2005)], and these show that the polyconvexity of a strain-energy function ensures the existence of global minimizers for the total elastic energy. Indeed, some nonlinear isotropic materials such as neo-Hookean, Mooney-Rivlin, and Ogden models can be shown to satisfy this polyconvex condition; however, anisotropic materials appear to be more difficult to construct with such conditions. Therefore, a polyconvex orthotropic strain energy function using a generalized structural tensor, developed by Itskov et al. [Itskov and Aksel (2004)], is utilized for the accurate and robust modeling of clothing behavior. The material model is implemented in a four-node shell element in Abaqus/Standard (S4R type) via the UMAT user-subroutine. Both models are used to predict the outcome of uniaxial tensile tests and compute the contact pressure of clothing over the human body so that appropriate designs of forms of clothing with better degree of fitting to the body can be obtained. The advantages and usefulness of these models are discussed in this paper.

The remainder of this paper is organized as follows. Section 2 describes the formulation of the rebar layer model. Section 3 presents an overview of anisotropic hyperelastic modeling using the polyconvex strain energy function. Accordingly, the macroscopic continuum constitutive model that can suitably capture the mechanical behavior of cloth is presented. The material law is implemented into a shell element in the FEM code, Abaqus/Standard, via the UMAT user-subroutine. Section 4 describes the validation and comparison of the experimental data with data obtained by a numerical simulation of the contact pressure of clothing against human skin. Section 5 summarizes the conclusions of our study.

## 2 Formulation of rebar layer model

This section briefly describes the formulation of the rebar layer model used to represent the characteristics of woven fabrics. This material model is decomposed into two parts: isotropic matrix part and reinforced rebar part. The isotropic matrix part uses the neo-Hookean hyperelastic material model. The potential energy of the neo-Hookean hyperelastic model  $W_{\text{neo}}$  is expressed as

$$W_{\text{neo}} = C_{10}(\lambda_1^2 + \lambda_1^2 + \lambda_1^2 - 3). \quad (1)$$

where  $C_{10}$  is a material parameter and  $\lambda_i$  ( $i = 1, 2, 3$ ) are principal stretch ratios.  $\lambda_1^2 + \lambda_2^2 + \lambda_3^2$  is equivalent to the first strain invariant  $I_1$  that is explained in next section. Element-based rebars are used to define the uniaxial reinforcement along the warp and weft directions, as shown in Fig.1. The material properties of the rebars can be given by the hypoelastic model with Young's moduli  $E_{warp}$  and  $E_{weft}$  in the warp and weft directions, respectively. The stress-strain relationship of this rebar layer model is defined as

$$\sigma^\nabla = \mathbb{D}(\epsilon) : \epsilon^\nabla, \tag{2a}$$

or in indice notation as

$$\sigma_{ij}^\nabla = D_{ijkl} \epsilon_{kl}^\nabla, \tag{2b}$$

where  $\sigma$ ,  $\sigma_{ij}$  is the true or the Cauchy stress tensor,  $\epsilon$ ,  $\epsilon_{kl}$  is the true or the logarithmic strain tensor,  $\mathbb{D}$ ,  $D_{ijkl}$  is the 4th-order elasticity tensor and is a function of  $\epsilon$ ,  $\epsilon_{kl}$ ; the symbol  $\nabla$  implies the objective rate; and the double dot product “:” represents multiplication and summation across two indices  $k, l$  of  $D_{ijkl}$  and  $\epsilon_{kl}$ . The elasticity tensor  $\mathbb{D}$  is obtained by the superposition of the isotropic matrix and rebars, as given by:

$$D_{ijkl} = \frac{\partial^2 W_{neo}}{\partial \epsilon_{ij} \partial \epsilon_{kl}} + E_{warp} \delta_{1i} \delta_{1j} \delta_{1k} \delta_{1l} + E_{weft} \delta_{2i} \delta_{2j} \delta_{2k} \delta_{2l}, \tag{3}$$

$$\{i, j, k, l\} = \{1, 2, 3\}$$

where directions 1 and 2 denote the warp and weft directions, respectively, direction 3 is perpendicular to both the warp and the weft directions, and  $\delta_{ij}$  represents Kronecker's delta.  $E_{warp}$  and  $E_{weft}$  can take the form of a series in terms of  $\epsilon_{11}$  and  $\epsilon_{22}$ , respectively.

$$E_{warp} = \sum_{i=0}^N c_i \epsilon_{11}^i \tag{4}$$

$$E_{weft} = \sum_{i=0}^N d_i \epsilon_{22}^i \tag{5}$$

The material parameters  $C_{10}$ ,  $c_i$ ,  $N$ , and  $d_i$  ( $i = 1, \dots, 6$ ) are determined through uniaxial tensile tests in 3 directions: warp, weft, and bias. In this model, the interaction between the warp and the weft rebar is not considered directly, and the isotropic matrix determines the deformation in the directions perpendicular to the stretch by the Poisson effect. This rebar layer model is implemented via Abaqus/Standard, in which the isotropic matrix part is represented by the shell element S4R, and its

reinforcement is modeled with the corresponding rebar elements in the warp and weft directions.

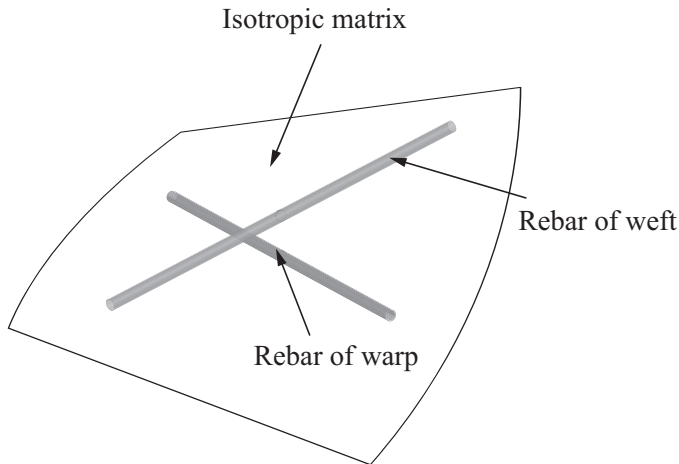


Figure 1: Schematic diagram of shell with rebar.

### 3 Formulation of anisotropic hyperelastic material model using polyconvex strain energy function

Although the abovedefined rebar layer model is quite easy to assemble and useful, it is not suitable for accurate fabric modeling of the interaction between warp and weft. To overcome this issue, another material model is proposed in this section. First, the polyconvexity condition of the strain energy function is outlined based on Schröder and Itskov's works [Schröder and Neff (2003b,a); Schröder, Neff, and Balzani (2005); Balzani, Neff, Schröder, and Holzapfel (2006); Balzani, Gruttmann, and Schröder (2008); Itskov and Aksel (2004); Itskov, Ehret, and Mavrilas (2006); Ehret and Itskov (2007)]. Next, the formulation of the anisotropic hyperelastic model is derived using the polyconvex strain energy function, and then, this formulation is used for modeling cloth. Finally, the implementation of the proposed models into the UMAT user-subroutine of Abaqus/Standard is discussed. Fundamentals of continuum mechanics, such as tensor calculations, finite rotations, finite deformations and objectivity, are basically referred to Atluri et al. [Rubinstein and Atluri (1983); Atluri (1984a,b)].

### 3.1 Polyconvexity of strain energy function

For a boundary value problem, the strain energy functions  $W$  are required to satisfy the four conditions listed below so that robust and reasonable analysis can be performed and a physically meaningful solution can be obtained. [Ball (1977); Hartmann and Neff (2003); Schröder and Neff (2003b); Schröder, Neff, and Balzani (2005); Itskov and Aksel (2004); Itskov, Ehret, and Mavrilas (2006)].

1. Continuity condition
2. Energy- and stress-free natural state condition
3. Polyconvexity condition
4. Growth condition

Condition 1 indicates that at least the  $C^2$ -continuity of the strain energy function should hold in order to compute the stress and tangent stiffness. Condition 2 refers to the necessity of an energy- and stress-free state in the reference configuration for a finite elasticity boundary value problem. Condition 3 is so defined that iff there exists a convex function  $W$  with respect to the deformation gradient tensor  $\mathbf{F}$ , cofactor of  $\mathbf{F}$  (denoted as  $\text{cof}\mathbf{F}$ ), and Jacobian  $J = \det\mathbf{F}$ , the strain energy function can be regarded as being polyconvex. Condition 4 refers to the coercivity. According to Ball [Ball (1977); Ball and Murat (1984)], the polyconvexity together with its continuity and coercivity is sufficient to ensure the existence of the global minimizer of the total elastic energy [Acerbi and Fusco (1984); Ball and Murat (1984); Müller, Qi, and Yan (1994); Steigmann (2003); Itskov and Aksel (2004)]. Morrey [Morrey (1952)] proved that the polyconvex strain energy functions satisfies the following ellipticity condition.

$$W = W(\mathbf{C}, \mathbf{M}_i), \tag{6}$$

$$\mathbf{H} : \frac{\partial^2 W}{\partial \mathbf{F} \partial \mathbf{F}} : \mathbf{H} \geq 0, \tag{7}$$

$$\mathbf{H} : \frac{\partial^2 W}{\partial \text{cof}\mathbf{F} \partial \text{cof}\mathbf{F}} : \mathbf{H} \geq 0, \tag{8}$$

$$\frac{\partial^2 W}{\partial J \partial J} \geq 0 \tag{9}$$

where  $\mathbf{H}$  is an arbitrary second-order tensor. Considering the abovementioned conditions, the strain energy function  $W$  of the anisotropic hyperelastic models can be

given in terms of the right Cauchy-Green deformation tensor  $\mathbf{C} = \mathbf{F}^T \mathbf{F}$  and a new tensor  $\mathbf{M}_i$  with the form:

$$W = W(\mathbf{C}, \mathbf{M}_i), \quad (10)$$

$\mathbf{M}_i$  are so-called structural tensors [Holzapfel (2000); Menzel and Steinmann (2001)] and they are denoted as

$$\mathbf{M}_i = \mathbf{n}_i \otimes \mathbf{n}_i, \quad (11)$$

$\mathbf{n}_i$  is the unit base vector in the principal material directions, as indicated by the simple 2D example shown in Fig.2, and  $\otimes$  represents the tensor product. Now,  $i$  represents the index of the fiber or the principal material direction, and the summation convention is not employed in this equation.

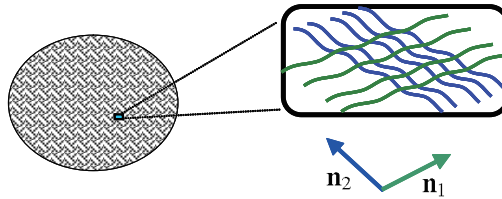


Figure 2: Structural tensor.

For orthotropic materials,  $\mathbf{n}_i \cdot \mathbf{n}_i = \delta_{ij}$  can be given, and  $\mathbf{M}_i$  has the following properties:

$$\sum_{i=1}^3 \mathbf{M}_i = \mathbf{I}, \quad (12)$$

$$\begin{cases} \mathbf{M}_i \mathbf{M}_j = \mathbf{0}, & i \neq j \\ \mathbf{M}_i \mathbf{M}_j = \mathbf{M}_i, & i = j \end{cases} \quad (13)$$

$$\text{tr} \mathbf{M}_i = 1, \quad (14)$$

where  $\mathbf{I}$  represents the second-order identity tensor. According to the material objectivity condition,  $W$  has to satisfy

$$W(\mathbf{C}, \mathbf{M}_i) = W(\mathbf{Q} \mathbf{C} \mathbf{Q}^T, \mathbf{Q} \mathbf{M}_i \mathbf{Q}^T), \quad (15)$$

where  $\mathbf{Q}$  is the orthogonal tensor that represents rigid rotation. According to the classical invariant theory,  $W$  in Eqn.(15) can be written based on (14) as

$$W = W(I_1, I_2, I_3, J_i, K_i), \tag{16}$$

where  $I_1, I_2$  and  $I_3$  represent the principal invariants of  $\mathbf{C}$  and they are given by

$$I_1 \equiv \text{tr} \mathbf{C} \tag{17}$$

$$I_2 \equiv \text{tr}(\text{cof} \mathbf{C}) \tag{18}$$

$$I_3 \equiv \det \mathbf{C} \tag{19}$$

$\text{cof}(\mathbf{C})$  is the cofactor of  $\mathbf{C}$ ; in the case of incompressible materials ( $I_3 = 1$ ),  $\text{cof}(\mathbf{C}) = \mathbf{C}^{-1}$  is satisfied.  $J_i$  and  $K_i$ , constructed using  $\mathbf{C}$  and  $\mathbf{M}_i$  represent the pseudo invariants of anisotropic materials. Schröder et al. advocated the use of the following definition of pseudo invariants because they can be convex with respect to  $\mathbf{F}$  and  $\text{cof} \mathbf{F}$ .

$$J_i \equiv \text{tr}(\mathbf{C}\mathbf{M}_i) = \mathbf{C} : \mathbf{M}_i. \tag{20}$$

$$K_i \equiv \text{tr}(\text{cof}(\mathbf{C})\mathbf{M}_i) = \text{cof}(\mathbf{C}) : \mathbf{M}_i. \tag{21}$$

Using these pseudo invariants, the polyconvex strain energy function can be constructed easily. In the next section, the results presented above are used to construct a polyconvex strain energy function that is applicable to clothing, subject to the four prerequisite conditions mentioned previously. In the implementation of a nonlinear FEM, the second Piola-Kirchhoff stress tensor  $\mathbf{S}$  and the fourth-order elasticity tensor  $\mathbb{C}$  should be calculated from the deformation state based on the strain energy function [Lu (2004)]  $W$  as

$$\mathbf{S} = 2 \frac{\partial W}{\partial \mathbf{C}}, \tag{22}$$

$$\mathbb{C} = 4 \frac{\partial^2 W}{\partial \mathbf{C} \partial \mathbf{C}}. \tag{23}$$

To compute Eqn.(22) and (23), the following tensor calculations are required:

$$\begin{aligned} \frac{\partial I_1}{\partial \mathbf{C}} &= \mathbf{I}, & \frac{\partial I_2}{\partial \mathbf{C}} &= I_1 \mathbf{I} - \mathbf{C}, & \frac{\partial I_3}{\partial \mathbf{C}} &= I_3 \mathbf{C}^{-1}, \\ \frac{\partial J_i}{\partial \mathbf{C}} &= \mathbf{M}_i, & \frac{\partial K_i}{\partial \mathbf{C}} &= -I_3 \mathbf{C}^{-1} \mathbf{M}_i \mathbf{C}^{-1} + K_i \mathbf{C}^{-1}. \end{aligned} \tag{24}$$

Note that the strain energy function has to satisfy the conditions of the energy- and stress-free natural state as follows:

$$\mathbf{S}|_{\mathbf{C}=\mathbf{I}} = \mathbf{0}. \tag{25}$$

### 3.2 Formulation of anisotropic hyperelastic model using polyconvex strain energy function for application to cloth

In this study, the following polyconvex strain energy function  $W$  for orthotropic incompressible hyperelastic materials, developed by Itskov [Itskov and Aksel (2004)], is utilized for modeling of cloth behavior.

$$W = \frac{1}{4} \sum_r^N \mu_r \left[ \frac{1}{\alpha_r} (\tilde{J}_r^{\alpha_r} - 1) + \frac{1}{\beta_r} (\tilde{K}_r^{\beta_r} - 1) \right]. \quad (26)$$

where  $N$ (positive integer),  $\mu_r > 0$ ,  $\alpha_r \geq 1$ , and  $\beta_r \geq 1$  are material constants, and  $\tilde{J}_r$  and  $\tilde{K}_r$  are generalized pseudo invariants defined as follows:

$$\tilde{J}_r \equiv \text{tr}(\mathbf{C}\tilde{\mathbf{M}}_r), \quad \tilde{K}_r \equiv \text{tr}(\text{cof}(\mathbf{C})\tilde{\mathbf{M}}_r), \quad (27)$$

where  $\tilde{\mathbf{M}}_r$  is the generalized structural tensor given by

$$\tilde{\mathbf{M}}_r \equiv w_1^{(r)} \mathbf{M}_1 + w_2^{(r)} \mathbf{M}_2 + w_3^{(r)} \mathbf{M}_3. \quad (28)$$

$w_i^{(r)}$  represent the weight factors of the principal material directions and  $w_i^{(r)}$  determine the effect of the interaction between fibers. The weight factors  $w_i^{(r)}$  take values between 0 and 1, as given in Eqn.(29), and the higher the value of  $w_i^{(r)}$ , the stronger is the effect of the fiber of direction  $i$  on others. This feature enables to obtain the expression of directional anisotropy. Note that when all  $w_i^{(r)}$  take values equal to 1/3, the material behaves as an isotropic one.

$$0 \leq w_i^{(r)} \leq 1. \quad (29)$$

The strain energy function satisfies the four prerequisite conditions mentioned in the previous section in such a manner that no additional restrictions should be imposed on the associated material coefficients. These coefficients can be further evaluated on the basis of experimental data.

### 3.3 Implementation in Abaqus/Standard UMAT

This section shows how the material model of Eqn.(26) is implemented in Abaqus/Standard by using the UMAT user-defined material subroutine. The present hyperelastic models need not have internal variables that are essential to history-dependent materials. Then, only components of the Cauchy stress and the tangent stiffness matrix, called as "material Jacobian" in Abaqus/Standard, are required to

return to the calling program. This is a convenient way to formulate the present material models with the total Lagrangian description associated with the second Piola-Kirchhoff stress given in Eqn.(22). On the other hand, Abaqus/Standard uses the updated Lagrangian description. Although the total and updated Lagrangian formulations are superficially different from each other, the underlying mechanics of the two are identical. Therefore, appropriate push-forward operations from the referred configurations to the current ones should be accounted for [Pinsky, Ortiz, and Karl S. Pister (1983); Meyers, Xiao, and Bruhns (2006); Zhang (2009)]. The second Piola-Kirchhoff stress  $\mathbf{S}$  can be transformed to the Cauchy stress  $\boldsymbol{\sigma}$  by the push-forward operation

$$\boldsymbol{\sigma} = \frac{1}{J} \mathbf{F} \mathbf{S} \mathbf{F}^T. \tag{30}$$

To specify the material Jacobian correctly, the component values have to be chosen and computed depending on the type of finite element and objective stress rate being used. Abaqus/Standard uses the Green-Naghdi rate of Kirchhoff stress  $\boldsymbol{\tau}^{\nabla G}$  and rate-of-deformation tensor  $\mathbf{D}$  for structural elements such as shells, membranes, beams, and trusses [Prot, Skallerud, and Holzapfel (2007) Abaqus (2008)]. Therefore, the tangent modulus  $\mathbb{C}^{\nabla G}$  related to the Green-Naghdi rate of the Kirchhoff stress tensor and rate-of-deformation tensor have to be given by the following expression:

$$\boldsymbol{\tau}^{\nabla G} = \mathbb{C}^{\nabla G} : \mathbf{D}. \tag{31}$$

Now, we derive  $\mathbb{C}^{\nabla G}$  from the elasticity tensor  $\mathbb{C}$  given in Eqn.(23). The Green-Naghdi rate of the Kirchhoff stress tensor  $\boldsymbol{\tau}^{\nabla G}$  is defined as

$$\boldsymbol{\tau}^{\nabla G} = \dot{\boldsymbol{\tau}} - \boldsymbol{\Omega} \boldsymbol{\tau} + \boldsymbol{\tau} \boldsymbol{\Omega}, \tag{32}$$

where  $\boldsymbol{\Omega} = \dot{\mathbf{R}} \mathbf{R}^T$  is the rigid spin tensor with  $\mathbf{R}$  denoting the rotation tensor. The tangent modulus  $\mathbb{C}^{\nabla J}$  between the Jaumann rate of the Kirchhoff stress tensor  $\boldsymbol{\tau}^{\nabla J}$  and  $\mathbf{D}$  is introduced as

$$\boldsymbol{\tau}^{\nabla J} = \dot{\boldsymbol{\tau}} - \mathbf{W} \boldsymbol{\tau} + \boldsymbol{\tau} \mathbf{W} = \mathbb{C}^{\nabla J} : \mathbf{D}, \tag{33}$$

where the superposed dot denotes the material time derivative and  $\mathbf{W}$  is the continuum spin tensor. Now, the material time derivative is employed in the Kirchhoff stress tensor  $\boldsymbol{\tau} = J \boldsymbol{\sigma} = \mathbf{F} \mathbf{S} \mathbf{F}^T$  as

$$\begin{aligned} \frac{d}{dt} \boldsymbol{\tau} &= \dot{\mathbf{F}} \mathbf{S} \mathbf{F}^T + \mathbf{F} \dot{\mathbf{S}} \mathbf{F}^T + \mathbf{F} \mathbf{S} \dot{\mathbf{F}}^T \\ &= (\mathbf{D} + \mathbf{W}) \boldsymbol{\tau} + \mathbf{F} \dot{\mathbf{S}} \mathbf{F}^T + \boldsymbol{\tau} (\mathbf{D} - \mathbf{W}). \end{aligned} \tag{34}$$

The Jaumann stress rate is derived by moving the terms of  $\mathbf{W}$  to the LHS in Eqn.(34) as

$$\begin{aligned}\dot{\boldsymbol{\tau}} - \mathbf{W}\boldsymbol{\tau} + \boldsymbol{\tau}\mathbf{W} &= \mathbf{F}(\mathbb{C} : \dot{\mathbf{E}})\mathbf{F}^T + \mathbf{D}\boldsymbol{\tau} + \boldsymbol{\tau}\mathbf{D}, \\ \boldsymbol{\tau}^{\nabla J} &= \mathbf{F}(\mathbb{C} : (\mathbf{F}^T \mathbf{D} \mathbf{F}))\mathbf{F}^T + \mathbf{D}\boldsymbol{\tau} + \boldsymbol{\tau}\mathbf{D},\end{aligned}\quad (35)$$

where  $\mathbf{E}$  is the Green-Lagrange strain tensor. Eqn.(35) is recast as the following expression using  $\mathbb{C}^{\nabla J}$  and  $\check{\mathbb{C}}$ :

$$\mathbb{C}^{\nabla J} : \mathbf{D} = \check{\mathbb{C}} : \mathbf{D} + \mathbf{D}\boldsymbol{\tau} + \boldsymbol{\tau}\mathbf{D}. \quad (36)$$

The above representation is rewritten in the form given below in terms of every component:

$$(\mathbb{C}^{\nabla J})_{ijkl} = (\check{\mathbb{C}})_{ijkl} + \tau_{ik}\delta_{jl} + \delta_{ik}\tau_{jl}, \quad (37)$$

where  $\check{\mathbb{C}}$  is the spatial elasticity tensor defined as

$$(\check{\mathbb{C}})_{ijkl} = F_{il}F_{jj}F_{kk}F_{lL}(\mathbb{C})_{IJKL}. \quad (38)$$

For the repeated indices  $I, J, K$ , and  $L$ , the summation convention is employed. The Jaumann stress rate and Green-Naghdi rate have the following relationship:

$$\boldsymbol{\tau}^{\nabla G} = \boldsymbol{\tau}^{\nabla J} + (\mathbf{W} - \boldsymbol{\Omega})\boldsymbol{\tau} - \boldsymbol{\tau}(\mathbf{W} - \boldsymbol{\Omega}). \quad (39)$$

Mehrabadi and Nemat-Nasser [Mehrabadi and Nemat-Nasser (1987)Simo and Hughes (1998)] derived the followingship relation between  $\mathbf{W}$  and  $\boldsymbol{\Omega}$ :

$$\mathbf{W} - \boldsymbol{\Omega} = \boldsymbol{\Lambda} : \mathbf{D}, \quad (40)$$

where  $\boldsymbol{\Lambda}$  is a fourth-order tensor represented as given below in the component-based form:

$$\Lambda_{ijkl} = \frac{1}{I_V II_V - III_V} \{ I_V^2 (V_{ik}\delta_{jl} - \delta_{ik}V_{jl}) - I_V (B_{ik}\delta_{jl} - \delta_{ik}B_{jl}) + B_{ik}V_{jl} - V_{ik}B_{jl} \}, \quad (41)$$

where  $B_{ij}$  is the left Cauchy-Green deformation tensor;  $V_{ij}$  is the left stretch tensor; and  $I_V$ ,  $II_V$ , and  $III_V$  are the principal invariants of  $V_{ij}$ . Consequently, the tangent modulus  $\mathbb{C}^{\nabla G}$  becomes

$$(\mathbb{C}^{\nabla G})_{ijkl} = (\mathbb{C}^{\nabla J})_{ijkl} + \Lambda_{iakl}\tau_{aj} - \tau_{ia}\Lambda_{ajkl}. \quad (42)$$

Note that  $\Lambda_{ijkl}$  has the following properties:

$$\Lambda_{ijkl} \neq \Lambda_{jikl}, \tag{43}$$

$$\Lambda_{ijkl} \neq \Lambda_{ijlk}, \tag{44}$$

$$\Lambda_{ijkl} = -\Lambda_{jilk}, \tag{45}$$

$$\Lambda_{ijkl} = \Lambda_{klij}. \tag{46}$$

By utilizing the above properties, the symmetric matrix for the material Jacobian  $\mathbb{C}^{\nabla MG}$  that is required in Abaqus/Standard can be given as

$$(\mathbb{C}^{\nabla MG})_{abcd} = \frac{1}{J} [(\mathbb{C}^{\nabla J})_{abcd} + \frac{1}{2}(\Lambda_{aecd} + \Lambda_{aedc})\tau_{eb} - \tau_{ae}\frac{1}{2}(\Lambda_{ebcd} + \Lambda_{ebdc})]. \tag{47}$$

To implement the derived material model in the shell elements, the additional plane stress condition and appropriate thickness update should be accounted for [Başar and Ding (1996, 1997); Başar and Itskov (1998); Başar, Itskov, and Eckstein (2000); Itskov (2001)]. In this study, an incompressible deformation is assumed for the current model to simplify the calculation of the thickness change. The initial thickness is 1 mm. The component of the deformation tensor in the thickness direction  $F_{33}$  is replaced with in-plane variables in the following manner:

$$F_{33} = \frac{1}{F_{11}F_{22} - F_{12}F_{21}}. \tag{48}$$

For incompressible materials, indeterminate hydrostatic pressure  $p$  occurs in the stress response as

$$\mathbf{S} = 2\frac{\partial W}{\partial \mathbf{C}} + p\mathbf{C}^{-1}. \tag{49}$$

Note that  $p$  can be eliminated at the element level via the plane stress condition  $S_{33} = 0$  to yield

$$p = -2\frac{\partial W}{\partial C_{33}}. \tag{50}$$

After substituting Eqn.(50) in Eqn.(49), we can obtain the stress tensor by considering the plane stress condition. The elasticity tensor related to this stress tensor can be derived by computing Eqn.(23). In this study,  $w_3^{(r)} = 0$  is employed by taking a zero fiber in the thickness direction. The transverse shear stiffness of the section

of a shear flexible shell element (such as S4R) in Abaqus/Standard is defined as follows [Abaqus (2008); Ma, Lu, Harbaugh, and Raghavan (2007)].

$$K_{11}^{ts} = \frac{5}{6}G_{13}t, \quad K_{22}^{ts} = \frac{5}{6}G_{23}t, \quad K_{12}^{ts} = 0, \quad (51)$$

where  $K_{11}^{ts}$ ,  $K_{22}^{ts}$ , and  $K_{12}^{ts}$  are the transverse shear stiffnesses;  $G_{13}$  and  $G_{23}$  are the material's shear moduli in the out-of-plane direction; and  $t$  is the thickness. The transverse shear stiffness should be specified as the initial, linear elastic stiffness of the shell in response to pure transverse shear strains. For the current model, the material's shear moduli are derived as

$$G_{13} = \frac{1}{2} \sum_i^N \mu_i w_1^{(i)}, \quad G_{23} = \frac{1}{2} \sum_i^N \mu_i w_2^{(i)}. \quad (52)$$

#### 4 Conditional provision and performing simulation to measure contact pressure of clothing

##### 4.1 Parameter identification of strain energy function

In this section, the material parameters to be assigned to the strain energy function given by Eqn.(26) are numerically identified so that the mechanical behavior of cloth can be predicted. The cloths considered in this study are made of knitted fabrics. Assuming that knitted fabrics behave like an orthotropic material in a macroscopic view, the anisotropy of the material is characterized by two families of yarns, i.e., warp and weft, as shown in Fig.3.

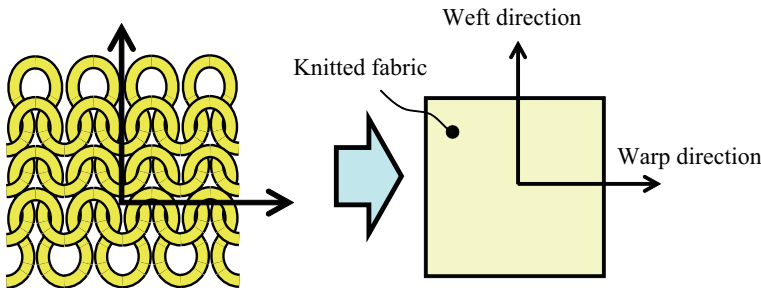
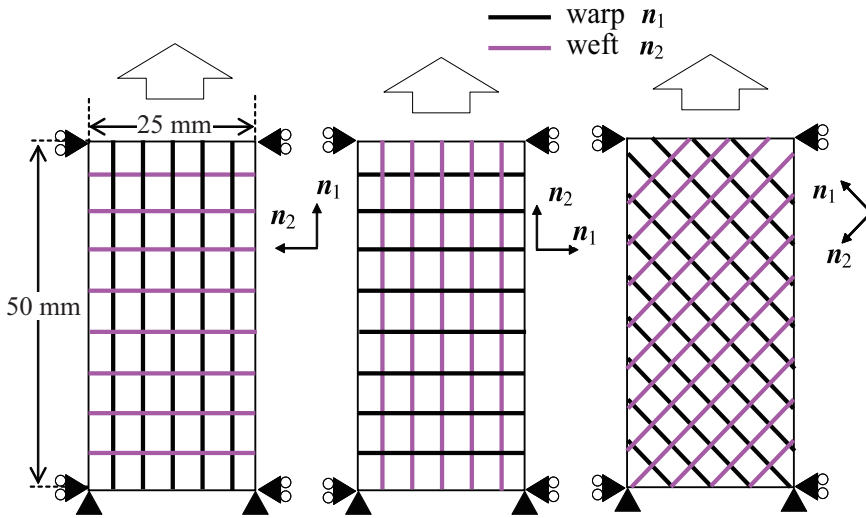


Figure 3: Schematic model of knitted fabric.



(a) Warp direction (b) Weft direction (c) Bias direction

Figure 4: Analysis model for simple tension of knitted strips of cloth.

To identify the material parameters in Eqn.(26), three uniaxial loadings in three directions: warp, weft, and bias at an angle of  $45^\circ$  are considered, as shown in Fig.4. To fit the load-displacement relationships with the experimental data in all three directions, the following objective function  $S$  in Eqn.(54) is minimized with respect to the material constants  $\mu_r$ ,  $\alpha_r$ ,  $\beta_r$ ,  $w_1^{(r)}$  and  $w_2^{(r)}$  subject to satisfying Eqn.(53) using Real-Coded GA [Sakuma and Kobayashi (2004)].

$\min S$

$$\begin{aligned} \text{s.t.} \quad & \mu_r \geq 0, \quad \alpha_r \geq 1, \quad \beta_r \geq 1, \\ & 0 \leq w_1^{(r)}, w_2^{(r)} \leq 1, \quad w_1^{(r)} + w_2^{(r)} = 1, \end{aligned} \quad (53)$$

$$S = \sum_{i=1}^l [\bar{t}_i - t(\bar{\lambda}_i)]^2 + \sum_{i=1}^m [\bar{t}_i - t(\bar{\lambda}_i)]^2 + \sum_{i=1}^n [\bar{t}_i - t(\bar{\lambda}_i)]^2, \quad (54)$$

where  $t$  is the nominal stress;  $\lambda$  is the stretch; and  $l$ ,  $m$ , and  $n$  are the number of experimental data points in the warp, weft, and bias directions, respectively.  $i$  indicates the sampling number and the overbar represents experimental values.  $t(\bar{\lambda}_i)$

denotes the  $i$ -th nominal stress calculated by the FEM.  $N$  in Eqn.(26) is set to 3 in this study. Now, the numerical identification of spats can be processed. Using the abovementioned method, the material parameters can be determined as shown in Table 1 for the rebar layer model and Table 2 for an anisotropic hyperelastic material. Fig.5 shows the load-displacement curve and deformation configurations in

Table 1: Material parameters of spats for rebar layer model.

$C_{10}$					
$8.4667 \times 10^{-3}$ MPa					
$c_0$	$c_1$	$c_2$	$c_3$	$c_4$	$c_5$
0.0001 MPa	0.1672 MPa	-2.225 MPa	21.199 MPa	-62.05 MPa	61.746 MPa
$d_0$	$d_1$	$d_2$	$d_3$	$d_4$	$d_5$
0.0032 MPa	-0.075 MPa	0.4653 MPa	-1.340 MPa	1.9400 MPa	-0.986 MPa

Table 2: Material parameters of spats for anisotropic hyperelastic model.

$\mu_1$		$\mu_2$		$\mu_3$	
$1.2755 \times 10^{-2}$ MPa		$2.0569 \times 10^{-3}$ MPa		$4.5867 \times 10^{-2}$ MPa	
$\alpha_1$	$\alpha_2$	$\alpha_3$	$\beta_1$	$\beta_2$	$\beta_3$
4.727	1.475	1.736	1.003	16.16	1.063
$w_1^{(1)}$	$w_2^{(1)}$	$w_1^{(2)}$	$w_2^{(2)}$	$w_1^{(3)}$	$w_2^{(3)}$
0.771	0.229	0.585	0.415	0.652	0.348

the warp, weft, and bias directions for the material parameters listed in Table 1 and Table 2. As shown in Fig.5, the resultant progress of deformation in the anisotropic hyperelastic model accurately matches the experimentally observed deformations and load-displacement responses in all cases with the optimized material parameters, whereas the rebar layer model exhibits the opposite deformation modes in the warp and weft directions, and a much lower load-displacement curve in the bias direction.

#### 4.2 Simulation that measures contact pressure of clothing

With this material model, a three-dimensional finite element analysis is carried out using Abaqus/Standard to obtain the distribution of clothing pressure acting on human skin. The material model is implemented via the UMAT user-subroutine for a user-defined material. This simulation aims to investigate the design of cloth that fits the human body. Cloth is meshed with four-noded shell elements (S4R in Abaqus/Standard) and the T-shirt fabrics are used in this simulation. The material parameters of the T-shirts are determined by the numerical identification mentioned

in the previous section as listed in Table 3 for the rebar layer model and Table 4 for the anisotropic hyperelastic model.

Table 3: Material parameters of T-shirts for rebar layer model.

$C_{10}$	$c_0$	$c_1$	$c_2$	$c_3$
$3.82 \times 10^{-2}$ MPa	0.0064 MPa	0.0786 MPa	-0.287 MPa	0.2156 MPa
$d_0$	$d_1$	$d_2$	$d_3$	
-0.010 MPa	0.0206 MPa	0.0291 MPa	-0.013 MPa	

Table 4: Material parameters of T-shirts for anisotropic hyperelastic model.

$\mu_1$	$\mu_2$		$\mu_3$		
$6.8837 \times 10^{-3}$ MPa	$8.6240 \times 10^{-2}$ MPa		$1.2354 \times 10^{-1}$ MPa		
$\alpha_2$	$\alpha_3$	$\alpha_3$	$\beta_1$	$\beta_2$	$\beta_3$
3.52	1.28	1.00	1.004	13.49	1.002
$w_1^{(1)}$	$w_2^{(1)}$	$w_1^{(2)}$	$w_2^{(2)}$	$w_1^{(3)}$	$w_2^{(3)}$
0.321	0.565	0.585	0.435	0.781	0.219

Fig.6 shows the load-displacement curves derived from the analysis using the material parameters listed in Table 3 and Table 4.

The results obtained from the abovementioned experimental method and the solutions derived from the FEM analysis are summarized here. The virtual human body model used in this simulation corresponds to an average body of a 20-year-old Japanese woman, as shown in Fig.7. An air-pressure measurement device is used to extract experimental data of the pressure. This system measures the clothing pressure by calculating the difference between the atmospheric pressure and the pressure pneumatically transmitted from the air packs attached to various positions on the body where the clothing contacts the skin. Therefore, this experimental system merely serves to obtain point-to-point measurement data through observation, and consequently, such an observation can hardly predict the overall distribution of contact pressure on the human skin. To overcome this difficulty, a numerical simulation using a nonlinear FEM is conducted to simulate the distribution of the contact pressure on the human body in the standing posture; this eliminates the need to design actual clothes. In this study, the human body is modeled by rigid elements. Because the surface of the dummy is sufficiently smooth to avoid the occurrence of any excessive tensions or wrinkles on the clothing during the experiment, the friction between the garment and the human body is not considered in the simulation. Fig.8 shows the process of the simulation that measures the contact pressure of clothing. As shown in Fig.8, the original shapes of the sewing patterns

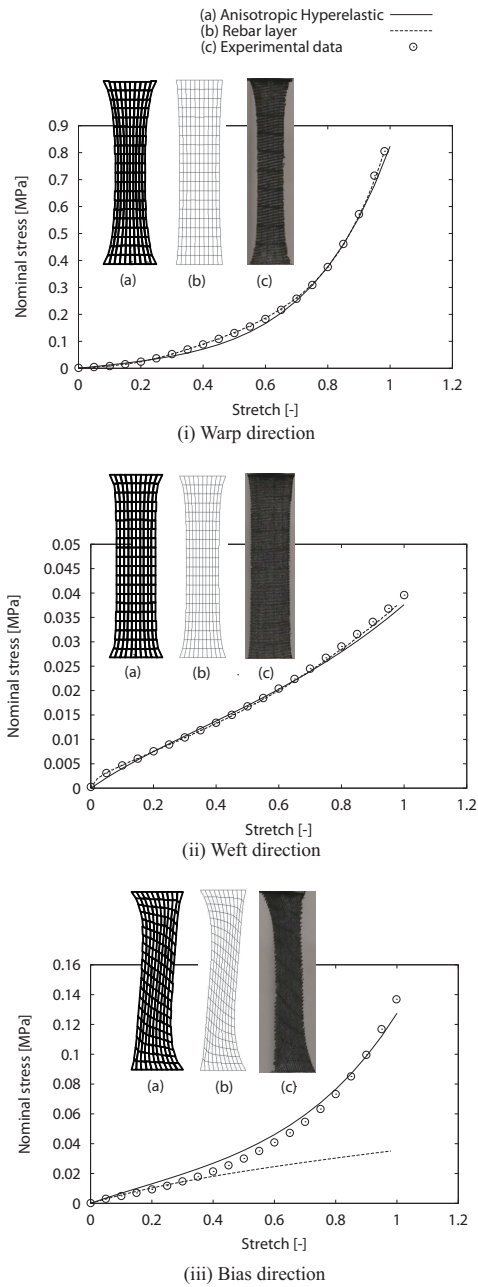


Figure 5: Load-displacement curves of spats in the warp, weft, and bias directions including deformation configurations.

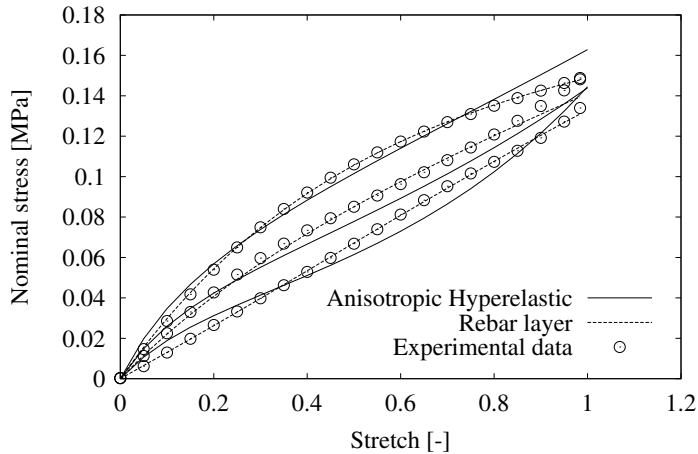
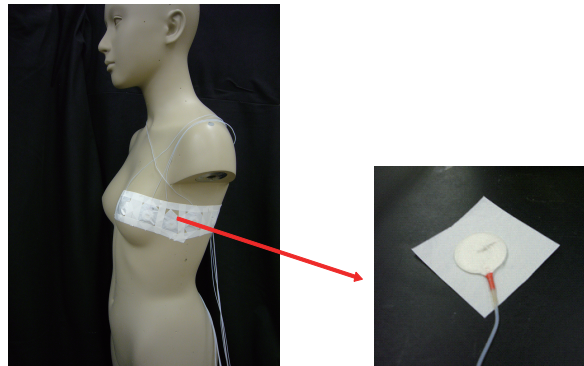


Figure 6: Load-displacement curves of T-shirts in the warp, weft, and bias directions.

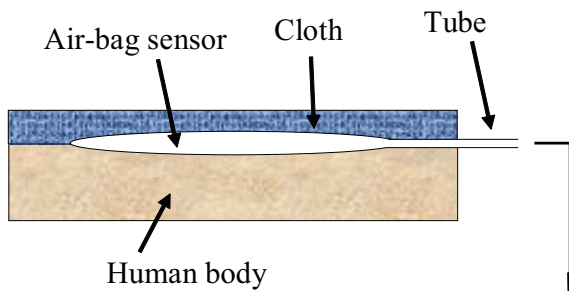
of clothes are first placed against the front and back of the body model, and then, these patterns are deformed so as to match the surface curves of the body to the greatest extent possible for the simulation to proceed. Fig.9 shows the contour of the contact pressure distributed over the human body surface. To validate the simulation results, a comparison is made with the experimental data extracted from the system shown in Fig.7 according to the sequence of points in the path, as shown in Fig.10. Fig.11 shows a comparison of the numerical data with the experimental ones. ①, ②, ... in Fig.11 denote the observation points shown in Fig.10. As noted in Fig.11, the numerical simulation with the anisotropic hyperelastic model is found to quantitatively be in good agreement with the experimental results. As compared to the results obtained with the rebar layer model, those obtained with the anisotropic hyperelastic model appear to better fit the measurement, especially under the armpit (at observation points ④ and ⑤). The validation and numerical efficiency of the anisotropic hyperelastic model are well demonstrated through this practical simulation.

## 5 Conclusion

This study presents the implementation of two material models to predict the mechanical behavior of cloth. One is the rebar layer model that consists of the isotropic hyperelastic matrix part and the reinforced rebar part. The other is the polyconvex anisotropic hyperelastic model; this model requires four conditions to be satisfied to



Air-bag pressure sensor



Pressure measurement device

Figure 7: Experiment system for contact pressure analysis.

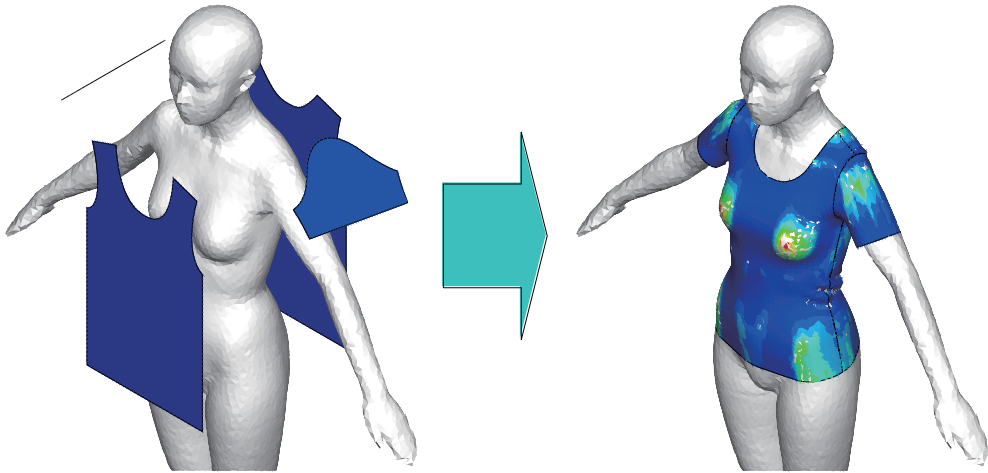


Figure 8: Procedure for simulation of contact pressure.

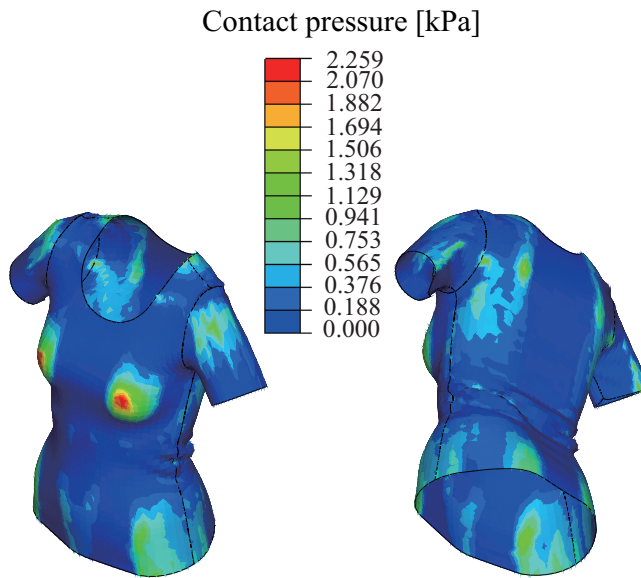


Figure 9: Contact pressure contour.

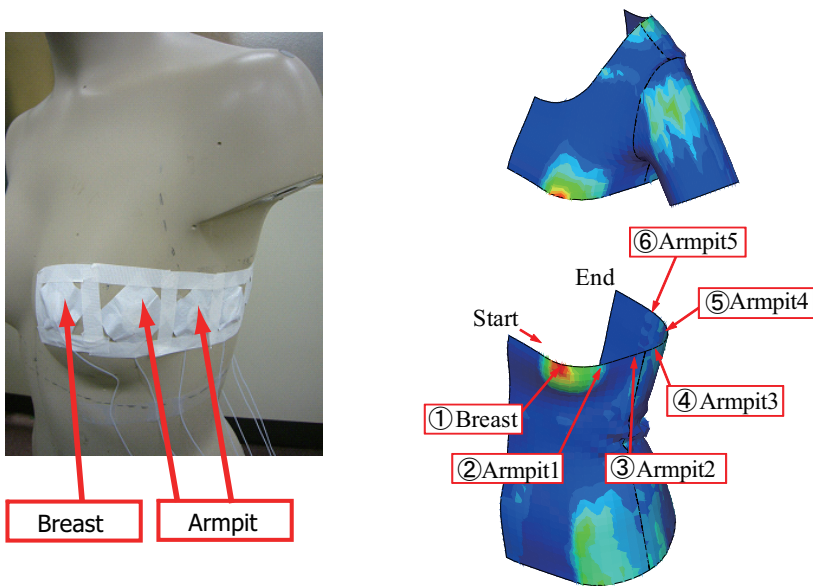


Figure 10: Measurement position of contact pressure.

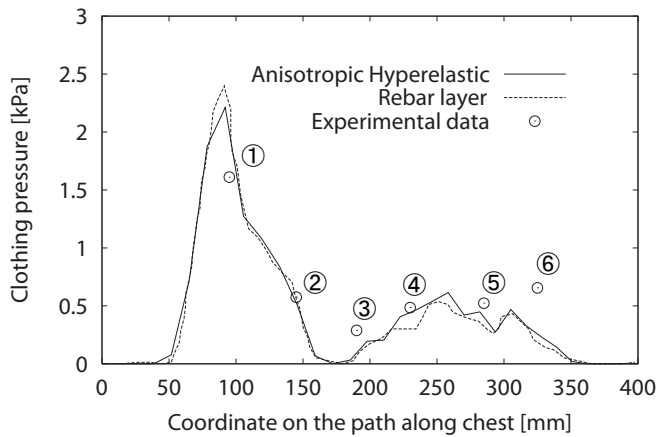


Figure 11: Comparison of contact pressure between analysis results and experimental results.

ensure the existence of the global minimizer of the total elastic energy of the body in boundary value problems, and the effect of the interaction between each fiber is considered for applying weight factors. The material parameters are numerically identified to fit the results to the experimental data of knitted strips stretched in the warp, weft, and bias directions. Using this material model, the simulation could successfully compute the pressure exerted by clothing on the human body model, and good agreement with the experimental data was realized. Through these researches, the following results are derived.

- The simulation of uniaxial tension tests for spats demonstrates the remarkable influence of anisotropy, and the polyconvex anisotropic hyperelastic model gives the load-displacement curves and deformation modes in better agreement with the experimental data in the warp, weft, and bias directions than the rebar layer model does.
- In the simulation of the clothing pressure distribution using T-shirts, the polyconvex anisotropic hyperelastic model gives more accurate results than the rebar layer model, especially for the armpits. Although the material of T-shirts demonstrates less influence of anisotropy than spats in tension tests, the biaxiality of the deformation gradient is more likely to appear in the armpits, and the polyconvex anisotropic hyperelastic model that considers the effect of interaction between the warp and the weft works better than the rebar layer model does in this part.

The validation and numerical efficiency of the models developed through this study are discussed in detail through the abovementioned simulation that measures the contact pressure of clothing. In the future, we intend to incorporate the biaxial tension test for woven fabric and the material model in our study.

**Acknowledgement:** The authors are grateful to Professor Junji Yoshida of the Yamanashi University for his considerable contributions with regard to Real-Coded GA. This research is strongly supported by the Technology Development Foundation for Rational Use of Energy (Next Generation Technology Development for Rational Use of Energy concerning Fabrics or Development of Fiber Products that induce Physical and Mental Comfort), in METI, Japan. This support is gratefully acknowledged. The late Professor Hirohisa Noguchi, a respected member of the Computational Mechanics Community, contributed greatly to this study until his untimely death on August 22, 2008.

## References

- Abaqus** (2008): *Abaqus Users Manual, Version 6.8, Dassault Systems Simulia Corp., USA, 2008.*
- Acerbi, E.; Fusco, N.** (1984): Semicontinuity problems in the calculus of variations. *Archive for Rational Mechanics and Analysis*, vol. 86, pp. 125–145.
- Atluri, S. N.** (1984): Alternate stress and conjugate strain measures, and mixed variational formulations involving rigid rotations, for computational analyses of finitely deformed plates and shells: Part-i: Thoery. *Computer & structure*, vol. 18, pp. 93–116.
- Atluri, S. N.** (1984): On constitutive relations at finite strain: Hypo-elasticity and elasto-plasticity with isotropic or kinematic hardening. *Computer Methods in Applied Mechanics and Engineering*, vol. 43, pp. 137–171.
- Başar, Y.; Ding, Y.** (1996): Finite-element analysis of hyperelastic thin shells with large strains. *Computatmnl Mechanics*, vol. 18, pp. 200–214.
- Başar, Y.; Ding, Y.** (1997): Shear deformation models for large-strain shell analysis. *International Journal of Solids and Structures*, vol. 34, pp. 1687–1708.
- Başar, Y.; Itskov, M.** (1998): Finite element formulation of the ogden material model with application to rubber-like shells. *International Journal for Numerical Methods in Engineering*, vol. 42, pp. 1279–1305.
- Başar, Y.; Itskov, M.; Eckstein, A.** (2000): Composite laminates: nonlinear interlaminar stress analysis by multi-layer shell elements. *Computer Methods in Applied Mechanics and Engineering*, vol. 185, pp. 367–397.
- Ball, J.** (1977): Convexity conditions and existence theorems in non-linear elasticity. *Archive for Rational Mechanics and Analysis*, vol. 63, pp. 337–403.
- Ball, J. M.; Murat, F.** (1984):  $w^{1,p}$ -quasiconvexity and variational problems for multiple integrals. *Journal of Functional Analysis*, vol. 58, pp. 225–253.
- Balzani, D.; Gruttmann, F.; Schröder, J.** (2008): Analysis of thin shells using anisotropic polyconvex energy densities. *Computer Methods in Applied Mechanics and Engineering*, vol. 197, pp. 1015–1032.
- Balzani, D.; Neff, P.; Schröder, J.; Holzapfel, G. A.** (2006): A polyconvex framework for soft biological tissues. adjustment to experimental data. *International Journal of Solids and Structures*, vol. 43, pp. 6052–6070.
- Bonet, J.; Burton, A. J.** (1998): A simple orthotropic, transversely isotropic hyperelastic constitutive equation for large strain computations. *Computer Methods in Applied Mechanics and Engineering*, vol. 162, pp. 151–164.

**Ehret, A. E.; Itskov, M.** (2007): A polyconvex hyperelastic model for fiber-reinforced materials in application to soft tissues. *Journal of Materials Science*, vol. 42, pp. 8853–8863.

**Harrysson, M.; Harrysson, A.; Ristinmaa, M.** (2007): Spatial representation of evolving anisotropy at large strains. *International Journal of Solids and Structures*, vol. 44, pp. 3514–3532.

**Hartmann, S.; Neff, P.** (2003): Polyconvexity of generalized polynomial-type hyperelastic strain energy functions for near-incompressibility. *International Journal of Solids and Structures*, vol. 40, pp. 2767–2791.

**Himpel, G.; Menzel, A.; Kuhl, E.; Steinmann, P.** (2007): Time-dependent fibre reorientation of transversely isotropic continua - finite element formulation and consistent linearization. *International Journal for Numerical Methods in Engineering*, vol. 73, pp. 1413–1433.

**Holzappel, G.** (2000): *Nonlinear Solid Mechanics: A Continuum Approach for Engineering*. Wiley.

**Ishimaru, S.; Isogai, Y.; Matsui, M.; Negishi, K.; Nonomura, C.; Yokoyama, A.** (2009): Prediction of clothing pressure distribution by using finite element method -1 -prediction of clothing pressure for pants. *Journal of Textile Engineering*, vol. 55, no. 6, pp. 179–186 (in Japanese).

**Itskov, M.** (2001): A generalized orthotropic hyperelastic material model with application to incompressible shells. *International Journal for Numerical Methods in Engineering*, vol. 50, pp. 1777–1799.

**Itskov, M.; Aksel, N.** (2004): A class of orthotropic and transversely isotropic hyperelastic constitutive models based on a polyconvex strain energy function. *International Journal of Solids and Structures*, vol. 41, pp. 3833–3848.

**Itskov, M.; Ehret, A. E.; Mavrilas, D.** (2006): A polyconvex anisotropic strain-energy function for soft collagenous tissues. *Biomech Model Mechanbiol*, vol. 5, pp. 17–26.

**Kwon, Y.; Roach, K.** (2004): Unit-cell model of 2/2-twillwoven fabric composites for multi-scale analysis. *CMES: Computer Modeling in Engineering & Sciences*, vol. 5, no. 1, pp. 63–72.

**Lu, J.** (2004): Exact expansions of arbitrary tensor functions  $\mathbf{F}(\mathbf{A})$  and their derivatives. *International Journal of Solids and Structures*, vol. 41, pp. 337–349.

**Lu, J.; Zhang, L.** (2005): Physically motivated invariant formulation for transversely isotropic hyperelasticity. *International Journal of Solids and Structures*, vol. 42, pp. 6015–6031.

- Lu, J.; Zhou, X.; Raghavan, M. L.** (2007): Computational method of inverse elastostatics for anisotropic hyperelastic solids. *International Journal for Numerical Methods in Engineering*, vol. 69, pp. 1239–1261.
- Ma, B.; Lu, J.; Harbaugh, R. E.; Raghavan, M. L.** (2007): Nonlinear anisotropic stress analysis of anatomically realistic cerebral aneurysms. *Transactions of the ASME*, vol. 129, pp. 88–96.
- Markert, B.; Ehlers, W.; Karajan, N.** (2005): A general polyconvex strain-energy function for fiber-reinforced materials. *Proceedings in Applied Mathematics and Mechanics*, vol. 5, pp. 245–246.
- Mehrabadi, M. M.; Nemat-Nasser, S.** (1987): Some basic kinematical relations for finite deformations of continua. *Mechanics of Materials*, vol. 6, pp. 127–138.
- Menzel, A.; Steinmann, P.** (2001): On the comparison of two strategies to formulate orthotropic hyperelasticity. *Journal of Elasticity*, vol. 62, pp. 171–201.
- Mesehke, G.; Helnwein, P.** (1994): Large-strain 3d-analysis of fibre-reinforced composites using rebar elements hyperelastic formulations for cords. *Computational Mechanics*, vol. 13, pp. 241–254.
- Meyers, A.; Xiao, H.; Bruhns, O. T.** (2006): Choice of objective rate in single parameter hypoelastic deformation cycles. *Computers & Structures*, vol. 84, pp. 1134–1140.
- Morrey, C. B.** (1952): Quasi-convexity and the lower semicontinuity of multiple integrals. *Pacific Journal of Mathematics*, vol. 2, pp. 25–53.
- Müller, S.; Qi, T.; Yan, B. S.** (1994): On a new class of elastic deformations not allowing for cavitation. *Annales de l'Institut Henri Poincaré (C) Analyse Non Linéaire*, vol. 11, no. 2, pp. 217–243.
- Nedjar, B.** (2007): An anisotropic viscoelastic fibre-matrix model at finite strains: Continuum formulation and computational aspects. *Computer Methods in Applied Mechanics and Engineering*, vol. 196, pp. 1745–1756.
- Pinsky, P. M.; Ortiz, M.; Karl S. Pister** (1983): Numerical integration of rate constitutive equation in finite deformation analysis. *Computer Methods in Applied Mechanics and Engineering*, vol. 40, pp. 137–158.
- Prot, V.; Skallerud, B.; Holzapfel, G.** (2007): Transversely isotropic membrane shells with application to mitral valve mechanics. constitutive modelling and finite element implementation. *International Journal for Numerical Methods in Engineering*, vol. 71, pp. 987–1008.

**Reese, S.; Raible, T.; Wriggers, P.** (2001): Finite element modelling of orthotropic material behaviour in pneumatic membranes. *International Journal of Solids and Structures*, vol. 38, pp. 9525–9544.

**Rubinstein, R.; Atluri, S. N.** (1983): Objectivity of incremental constitutive relations over finite time steps in computational finite deformation analyses. *Computer Methods in Applied Mechanics and Engineering*, vol. 36, pp. 227–290.

**Sakuma, J.; Kobayashi, S.** (2004): Real-coded ga for high-dimensional k-tablet structures. *Transactions of the Japanese Society for Artificial Intelligence*, vol. 19, no. 1, pp. 28–37.

**Schröder, J.; Neff, P.** (2003): Construction of polyconvex, anisotropic free-energy functions. *Proceedings in Applied Mathematics and Mechanics*, vol. 2, pp. 172–173.

**Schröder, J.; Neff, P.** (2003): Invariant formulation of hyperelastic transverse isotropy based on polyconvex free energy functions. *International Journal of Solids and Structures*, vol. 40, pp. 401–445.

**Schröder, J.; Neff, P.; Balzani, D.** (2005): A variational approach for materially stable anisotropic hyperelasticity. *International Journal of Solids and Structures*, vol. 42, pp. 4352–4371.

**Simo, J.; Hughes, T.** (1998): *Computational Inelasticity*. Springer.

**Steigmann, D. J.** (2003): On isotropic, frame-invariant, polyconvex strain-energy functions. *The Quarterly Journal of Mechanics and Applied Mathematics*, vol. 56, no. 4, pp. 483–491.

**ten Thije, R.; Akkerman, R.; Huétink, H.** (2007): Large deformation simulation of anisotropic material using an updated lagrangian finite element method. *Computer Methods in Applied Mechanics and Engineering*, vol. 196, pp. 3141–3150.

**Zhang, X. Q.** (2009): Objective stress rates and residual strains in stress cycles. *Multidiscipline Modeling in Materials and Structures*, vol. 5, pp. 77–98.